Strain-Based Regional Nonlinear Cardiac Material Properties Estimation From Medical Images

Ken C. L. Wong[1,2], Jatin Relan[2], Linwei Wang[1], Maxime Sermesant[2], Hervé Delingette[2], Nicholas Ayache[2], and Pengcheng Shi[1]

[1]Computational Biomedicine Laboratory, Rochester Institute of Technology, Rochester, USA
{chun.lok.wong, linwei.wang, pengcheng.shi}@rit.edu
[2]ASCLEPIOS Research Project, INRIA Sophia Antipolis, France
{jatin.relan, maxime.sermesant, herve.delingette, nicholas.ayache}@inria.fr

Abstract. Model personalization is essential for model-based surgical planning and treatment assessment. As alteration in material elasticity is a fundamental cause to various cardiac pathologies, estimation of material properties is important to model personalization. Although the myocardium is heterogeneous, hyperelastic, and orthotropic, existing image-based estimation frameworks treat the tissue as either heterogeneous but linear, or hyperelastic but homogeneous. In view of these, we present a physiology-based framework for estimating regional, hyperelastic, and orthotropic material properties. A cardiac physiological model is adopted to describe the macroscopic cardiac physiology. By using a strain-based objective function which properly reflects the change of material constants, the regional material properties of a hyperelastic and orthotropic constitutive law are estimated using derivative-free optimization. Experiments were performed on synthetic and real data to show the characteristics of the framework.

1 Introduction

Estimation of subject-specific cardiac deformation has been an active research area for decades as it provides useful information for verifying location and extent of cardiac diseases [1]. Nevertheless, for model-based surgical planning, treatment assessment, and cardiology study, retrieval of subject-specific cardiac physiological parameters is necessary [2]. As alterations in myocardial fiber structure and material elasticity are the more fundamental causes to various cardiac pathologies [3], estimation of material properties is important for model personalization.

Although many works have studied myocardial material characteristics through biomechanics [3], estimation of *in vivo* and subject-specific material properties is better realized through medical images. In [4], homogeneous, piecewise linear, and transversely isotropic material constants were estimated together with active stresses using tagged magnetic resonance images (MRI). In [5], a simultaneous motion and material properties estimation framework was developed to estimate heterogeneous, linear, and isotropic material constants from phase contrast and tagged MRI. Although these works show physiologically and clinically interesting results, the use of linear material models may be physiologically implausible as the myocardial tissue is hyperelastic and orthotropic [3, 6]. The estimation of hyperelastic material constants from images

was unavailable until recently. In [7, 8], homogeneous, hyperelastic, and transversely isotropic material properties were estimated. A finite deformation elasticity problem was solved for early diastolic filling to simulate the passive mechanics of the left ventricle, and the estimation was performed by matching the predicted motion of material points derived from tagged MRI. Nevertheless, homogeneous properties are insufficient for model personalization. Furthermore, the interaction with active contraction was not accounted for in [5, 7, 8], and all frameworks used displacements as measurements.

In view of these issues, we present a physiology-based framework of estimating regional, hyperelastic, and orthotropic material properties from medical images. A cardiac physiological model comprising electric wave propagation and biomechanics is adopted [9]. Using a strain-based objective function which properly reflects the change of material constants, the regional exponential material constants of a hyperelastic and orthotropic constitutive law [6] are estimated through the BOBYQA algorithm for bound constrained optimization [10]. Although a cardiac cycle involves the interactions between active contraction, passive mechanics, and boundary conditions, to simplify the problem, we assume that the fibrous-sheet structure, active contraction, and boundary conditions are given and to be investigated in other papers. Experiments were performed on synthetic and real data to show the characteristics of the framework.

2 Cardiac Material Properties Estimation

2.1 Cardiac Physiological Model

The cardiac physiological model comprises electric wave propagation and biomechanics, which relates active contraction with cardiac deformation through given material properties and boundary conditions. The total-Lagrangian dynamics is utilized [9]:

$$\mathbf{M}\ddot{\mathbf{U}} + \mathbf{C}\dot{\mathbf{U}} + \mathbf{K}\Delta\mathbf{U} = \mathbf{F} \tag{1}$$

where $\mathbf{M}$, $\mathbf{C}$, and $\mathbf{K}$ are the mass, damping, and stiffness matrices respectively. $\mathbf{F}$ comprises active forces from electric wave propagation [11], internal stresses caused by finite deformation, and also the displacement boundary conditions. $\ddot{\mathbf{U}}$, $\dot{\mathbf{U}}$ and $\Delta\mathbf{U}$ are the respective acceleration, velocity and incremental displacement vectors respectively. With (1), the cardiac deformation can be related to the material properties in $\mathbf{K}$.

2.2 Strain Energy Function

The material properties in $\mathbf{K}$ are characterized by the strain energy function in [6]:

$$\Psi(\boldsymbol{\epsilon}) = \kappa(J\ln J - J + 1) + \frac{1}{2}a(e^{Q} - 1) \tag{2}$$

where
$$\begin{aligned} Q =& b_{ff}\bar{\epsilon}_{ff}^2 + b_{ss}\bar{\epsilon}_{ss}^2 + b_{nn}\bar{\epsilon}_{nn}^2 \\ &+ b_{fs}\left(\bar{\epsilon}_{fs}^2 + \bar{\epsilon}_{sf}^2\right) + b_{fn}\left(\bar{\epsilon}_{fn}^2 + \bar{\epsilon}_{nf}^2\right) + b_{sn}\left(\bar{\epsilon}_{sn}^2 + \bar{\epsilon}_{ns}^2\right) \end{aligned} \tag{3}$$

with J the determinant of deformation gradient, and κ the penalty factor for tissue incompressibility. $\bar{\epsilon}_{ij}$ are the isovolumetric components of the Green-Lagrange strain tensor $\boldsymbol{\epsilon}$. a (kPa) and b_{ij} (unitless) are the material constants. The f-s-n coordinate system

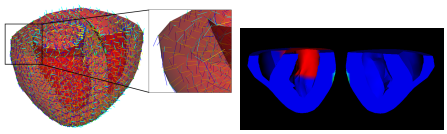

(a) Heart Representation.

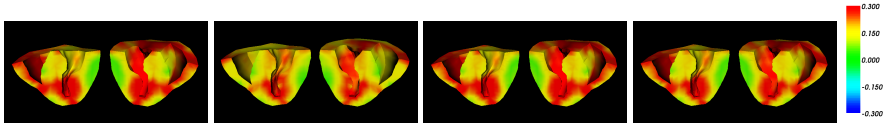

(b) First principal strains at end systole.

Fig. 1. Synthetic data. (a) Left: heart geometry and tissue structure (f,s,n: fiber, sheet, sheet normal: blue, yellow, cyan). Right: infarcted region shown in red. (b) Left to right: simulated ground truth, simulations with initial parameters, with parameters from MI-based metric, and with parameters from MSE-based metric.

represents the fibrous-sheet structure. With (2), the stress tensor and elasticity tensor can be derived and embedded into the cardiac electromechanical dynamics. Because of the difficulty in separating a from b_{ij} [6, 8], only b_{ij} are estimated in this paper.

2.3 Strain-Based Derivative-Free Optimization

As realistic cardiac material properties are nonlinear [3], estimating material constants from deformation is a nonlinear optimization problem. In [11], the adjoint method was used to estimate the local active contractility from cardiac deformation. In [5], a simultaneous motion and material properties estimation framework based upon the maximum a posteriori estimation principles was realized through the extended Kalman smoother. These frameworks linearize the objective functions through approximations and assumptions, which may reduce the physiological plausibility and stability of the system dynamics. Furthermore, as each change of the material constants affects the whole cardiac cycle, frame-to-frame updates of material constants in [5] may reduce the physiological plausibility of the estimation.

In consequence, the BOBYQA algorithm for derivative-free bound constrained optimization is utilized [10]. With $\boldsymbol{\theta}$ the parameters to be estimated, this algorithm approximates the objective function $\mathcal{F}(\boldsymbol{\theta})$ as a quadratic function, which is updated iteratively to search for the minimum within the given boundaries. As no linearization is performed, the intact nonlinearity of the model can be preserved. Furthermore, without the tedious derivation of the objective function gradient, more complicated but appropriate functions can be investigated. Our objective function is given as:

$$\mathcal{F}(\boldsymbol{\theta}) = \sum_{f} \sum_{r} \sum_{i} \sum_{j} g_r \left(\bar{\epsilon}_{ij}, \epsilon_{ij}(\boldsymbol{\theta}) \right) \tag{4}$$

with f and r the frames and regions used respectively. $\bar{\epsilon}_{ij}$ are the strain measurements from image-based cardiac motion recovery under the local f-s-n basis at region r [9],

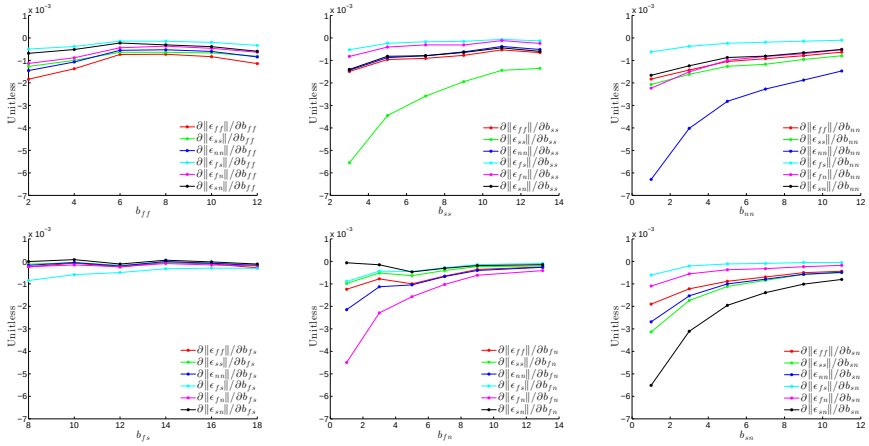

Fig. 2. Sensitivity analysis on synthetic data. Sensitivities of f-s-n Green-Lagrange strains with respect to b_{ij}. $\|\epsilon_{ij}\|$ are the mean strain magnitudes in a cardiac cycle.

Table 1. Synthetic data. Ground-truth parameters and estimated parameters. $a = 0.8$ kPa at the LV and RV and $a = 1.2$ kPa at the infarcted region.

	Ground truth						MI-based						MSE-based					
	b_{ff}	b_{ss}	b_{nn}	b_{fs}	b_{fn}	b_{sn}	b_{ff}	b_{ss}	b_{nn}	b_{fs}	b_{fn}	b_{sn}	b_{ff}	b_{ss}	b_{nn}	b_{fs}	b_{fn}	b_{sn}
LV	6.0	7.0	3.0	10.0	4.0	5.0	6.3	7.0	3.1	7.6	3.8	4.9	5.5	8.0	3.9	7.6	3.9	6.2
RV	5.0	6.0	2.0	9.0	3.0	4.0	5.0	6.2	1.6	8.3	3.5	3.8	3.4	6.8	2.2	8.7	3.0	4.1
Infarcted	8.0	9.0	5.0	12.0	6.0	7.0	8.4	8.2	5.7	10.8	5.5	6.8	7.6	7.4	6.8	8.1	6.3	7.4

and $\epsilon_{ij}(\boldsymbol{\theta})$ are the corresponding strains simulated using (1). This strain-based objective function better reflects the change of b_{ij} as shown in the sensitivity analysis in Section 3.1. $g_r(\bullet)$ computes the similarity between the measured and simulated strains in region r, for which the mean-squared-error-based (MSE-based) and the mutual-information-based (MI-based) metrics were investigated (Section 3.2 and 3.3). The MSE-based metric minimizes the absolute difference, while the MI-based metric minimizes the difference between patterns regardless of the local contrasts. With (4), assuming the active contraction and boundary conditions are given, b_{ij} are estimated simultaneously.

3 Experiments

3.1 Sensitivity Analysis

Strains ϵ_{ij} are direct components of strain energy functions (e.g. (3)) comprising spatial derivatives of displacements, thus are more appropriate for material properties estimation. To show the relations between ϵ_{ij} and b_{ij} under the local f-s-n basis, a sensitivity analysis was performed. The heart architecture from the University of Auckland was used to provide the anatomical cardiac geometry and tissue structure for the experiments [12] (Fig. 1(a)). With the parameters obtained from [6] ($a = 0.88$ kPa, $b_{ff} = 6$,

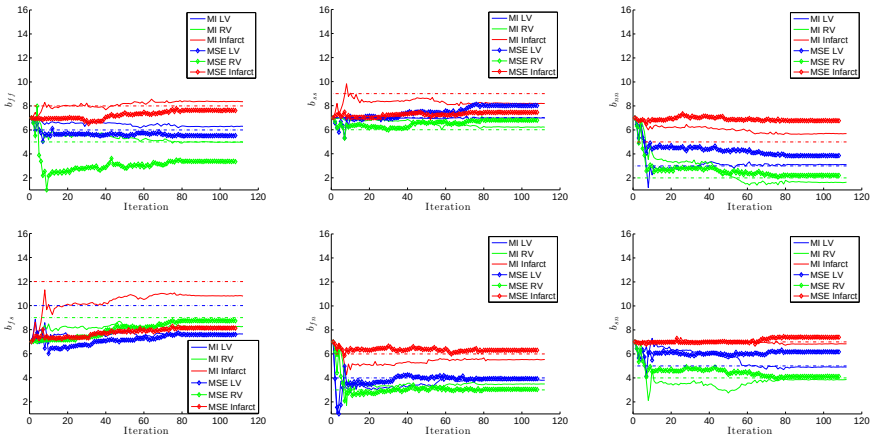

Fig. 3. Synthetic data. Parameter estimation using MI-based and MSE-based metrics. Blue, green, and red dash-dot lines represent the ground truths of LV, RV, and infarct.

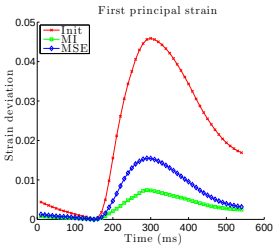

Fig. 4. Synthetic data. Mean deviations of first principal strains from the ground truth.

$b_{ss} = 7$, $b_{nn} = 3$, $b_{fs} = 12$, $b_{fn} = 3$, $b_{sn} = 3$), cardiac cycles with different parameters were simulated with normal electrical propagation through (1) for the one-at-a-time sensitivity analysis (Fig. 2) [13]. The results show that ϵ_{ij} are most sensitive when the corresponding b_{ij} changes, thus strain-based objective function is a proper choice for material properties estimation.

3.2 Synthetic Data

Experimental Setup The heart architecture from the University of Auckland was used (Fig. 1(a)). The heart was partitioned into regions of LV, RV, and infarct (Fig. 1(a)), with parameters shown in Table 1. A cardiac cycle of 550 ms was simulated using the cardiac physiological model as the ground truth, and the resulted strains were used as the measurements. The MI-based and MSE-based metrics of g_r in (4) were tested. In the experiments, a is known, and b_{ij} were initialized as 7 and were estimated simultaneously using the measurements from the whole cardiac cycle.

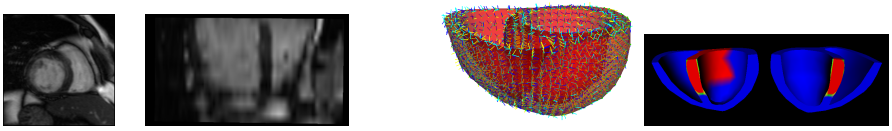

(a) MRI. (b) Heart representation.

Fig. 5. Real data. (a) MRI. (b) Left: tissue structures (f,s,n: fiber, sheet, sheet normal: blue, yellow, cyan). Right: infarcted region shown in red.

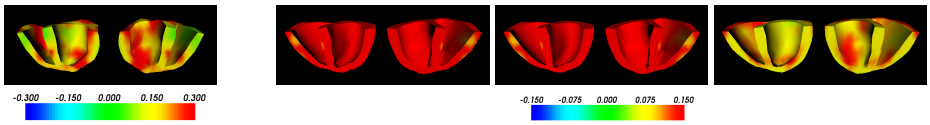

(a) (b)

Fig. 6. Real data. First principal strains at end systole. (a) Recovered cardiac deformation from MRI. (b) Left to right: simulations with initial parameters, with parameters from MI-based metric, and with parameters from MSE-based metric.

Results Fig. 3 shows the material constants at each iteration during optimization, and Table 1 shows the estimated material constants. Comparing between the MI-based and MSE-based metrics, they have similar numbers of iterations before convergence, but the MI-based metric gives better parameter identification. For both metrics, except b_{fs}, the estimated b_{ij} maintain the correct regional orders. Such orders appeared at the early iterations, and the latter iterations refined the results. The performance of estimating b_{fs} can be inferred from the sensitivity analysis (Fig. 2), in which the strains are less sensitive to b_{fs}. Fig. 1(b) shows the cardiac deformation at end systole. Although the MSE-based metric has less accurate estimation, the simulation using the corresponding parameters is very close to the ground truth, and is similar to the simulation using the parameters estimated by the MI-based metric (Fig. 4).

3.3 Real Data

Experimental Setup To investigate the behaviors of the proposed framework in reality when the tissue structure, active contraction, and boundary conditions are not ideal, experiments were performed on human data sets from patients with acute myocardial infarction [14]. Because of the page limits, only the results of Case 2 are presented. Case 2 contains a human short-axis MRI sequence of 16 frames (50 ms/frame), 13 slices/frame, 8 mm inter-slice spacing, and in-plane resolution 1.32 mm/pixel (Fig. 5(a)). Segmentation was performed to obtain the initial heart geometry, with the fibrous-sheet structure mapped from the Auckland heart architecture using nonrigid registration (Fig. 5(b)). The expert-identified infarcted region is shown in Fig. 5(b), and the heart geometry was partitioned into LV, RV, and infarct accordingly. The cardiac deformation was estimated from the MRI sequence using the framework in [9] to provide the strain inputs for the material properties estimation. Active contraction parameters were adopted from the lit-

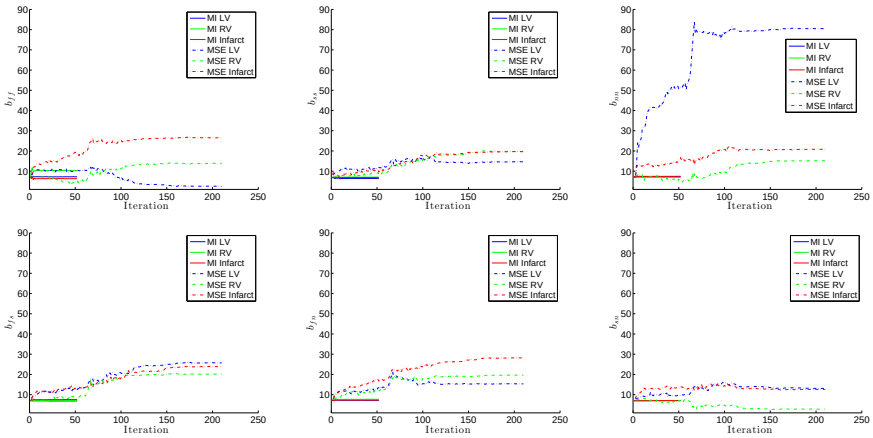

Fig. 7. Real data. Parameter estimation using MI-based and MSE-based metrics.

Table 2. Real data. Estimated parameters. $a = 0.88$ kPa at all regions.

	MI-based						MSE-based					
	b_{ff}	b_{ss}	b_{nn}	b_{fs}	b_{fn}	b_{sn}	b_{ff}	b_{ss}	b_{nn}	b_{fs}	b_{fn}	b_{sn}
LV	7.2	6.4	7.3	6.9	7.2	7.1	2.6	14.7	80.5	25.7	15.3	13.1
RV	10.3	7.1	6.9	7.1	7.7	7.1	13.9	19.7	15.2	20.1	19.6	2.8
Infarcted	6.3	6.8	7.5	7.6	7.3	7.1	26.6	19.7	20.9	23.9	28.2	12.6

erature [3, 11] but manually calibrated using the recovered cardiac cycle with the initial material constants. $a = 0.88$ kPa at all regions, and b_{ij} were initialized as 7 and were estimated simultaneously.

Results Fig. 7 shows the material constants at each iteration during optimization, and Table 2 shows the estimated material constants. For the real data, the performances between the MI-based and MSE-based metrics are very different. The MI-based metric did not have proper estimation of parameters, which only slightly fluctuate around the initial value of 7 until convergence. On the other hand, the MSE-based metric performed much better. Except the outlier of b_{nn} at the LV which is probably caused by the unrealistic active contraction and boundary conditions, other parameters evolved in the range similar to those in other researches [7, 8], and the estimated parameters can partially reflect the properties of the infarcted region. Fig. 6 shows the visual comparisons at end systole. The simulated strain pattern using the parameters from the MI-based metric is very similar to that of the initialization which deviates a lot from the measured strain from the MRI. On the other hand, although the strain simulated using the parameters from the MSE-based metric is only halved of that of the measurements, the strain pattern properly accounts for the infarcted region.

4 Discussions

The experiments on the synthetic data show that in the ideal situation, the performance of MSE-based and MI-based metrics are similar, and the MI-based metric gives better results. Nevertheless, the results on the real data show that when the discrepancies between simulations and measurements are large because of the improper tissue structure, active contraction, and boundary conditions, the use of MI-based metric is less robust, though more experiments are required to confirm this justification.

References

1. Frangi, A.J., Niessen, W.J., Viergever, M.A.: Three-dimensional modeling for functional analysis of cardiac images: a review. IEEE Transactions on Medical Imaging **20**(1) (2001) 2–25
2. Hunter, P.J.: Modeling human physiology: the IUPS/EMBS physiome projec. Proceedings of the IEEE **94**(4) (2006) 678–691
3. Glass, L., Hunter, P., McCulloch, A., eds.: Theory of Heart: Biomechanics, Biophysics, and Nonlinear Dynamics of Cardiac Function. Springer-Verlag (1991)
4. Hu, Z., Metaxas, D., Axel, L.: *In vivo* strain and stress estimation of the heart left and right ventricles from MRI images. Medical Image Analysis **7**(4) (2003) 435–444
5. Liu, H., Shi, P.: Maximum a posteriori strategy for the simultaneous motion and material property estimation of the heart. IEEE Transactions on Biomedical Engineering **56**(2) (2009) 378–389
6. Usyk, T.P., Mazhari, R., McCulloch, A.D.: Effect of laminar orthotropic myofiber architecture on regional stress and strain in the canine left ventricle. Journal of Elasticity **61** (2000) 143–164
7. Wang, V.Y., Lam, H.I., Ennis, D.B., Cowan, B.R., Young, A.A., Nash, M.P.: Modelling passive diastolic mechanics with quantitative MRI of cardiac structure and function. Medical Image Analysis **13**(5) (2009) 773–784
8. Xi, J., Lamata, P., Shi, W., Niederer, S., Land, S., Rueckert, D., Duckett, S.G., Shetty, A.K., Rinaldi, C.A., Razavi, R., Smith, N.: An automatic data assimilation framework for patient-specific myocardial mechanical parameter estimation. In: International Conference on Functional Imaging and Modeling of the Heart. Volume 6666 of LNCS., Springer (2011) 392–400
9. Wong, K.C.L., Wang, L., Zhang, H., Liu, H., Shi, P.: Physiological fusion of functional and structural images for cardiac deformation recovery. IEEE Transactions on Medical Imaging **30**(4) (2011) 990–1000
10. Powell, M.J.D.: The BOBYQA algorithm for bound constrained optimization without derivatives. Technical report, DAMTP, University of Cambridge (2009)
11. Sermesant, M., Moireau, P., Camara, O., Sainte-Marie, J., Andriantsimiavona, R., Cimrman, R., Hill, D.L.G., Chapelle, D., Razavi, R.: Cardiac function estimation from MRI using a heart model and data assimilation: advances and difficulties. Medical Image Analysis **10** (2006) 642–656
12. LeGrice, I.J., Smaill, B.H., Chai, L.Z., Edgar, S.G., Gavin, J.B., Hunter, P.J.: Laminar structure of the heart: ventricular myocyte arrangement and connective tissue architecture in the dog. Am J Physiol Heart Circ Physiol **269** (1995) H571–H582
13. Saltelli, A., Ratto, M., Andres, T., Campolongo, F., Cariboni, J., Gatelli, D., Saisana, M., Tarantola, S.: Global Sensitivity Analysis: The Primer. John Wiley & Sons Ltd (2008)
14. PhysioNet/Computers in Cardiology challenge 2007: electrocardiographic imaging of myocardial infarction. http://www.physionet.org/challenge/2007/